Biomaterials Science

# Designing nanoparticle carriers for enhanced drug efficacy in photodynamic therapy



| | |
|---|---|
| Journal: | *Biomaterials Science* |
| Manuscript ID: | BM-ART-01-2014-000024.R1 |
| Article Type: | Paper |
| Date Submitted by the Author: | 17-Feb-2014 |





| | |
|---|---|
| Complete List of Authors: | Chu, Zhiqin; The Chinese University of Hong Kong, Physics Department<br>Zhang, Silu; The Chinese University of Hong Kong, Physics Department<br>Yin, Chun; The Chinese University of Hong Kong, School of Biomedical Sciences<br>LIN, Ge; The Chinese University of Hong Kong, Hong Kong, School of Biomedical Sciences<br>Li, Quan; The Chinese University of Hong Kong, Department of Physics |

Journal Name

RSCPublishing

ARTICLE

# Designing nanoparticle carriers for enhanced drug efficacy in photodynamic therapy

Cite this: DOI: 10.1039/x0xx00000x

Zhiqin Chu[a†], Silu Zhang[a†], Chun Yin[b], Ge Lin[b], Quan Li[a*]

Received ooth January 2012,
Accepted ooth January 2012

DOI: 10.1039/x0xx00000x

www.rsc.org/

Although nanoparticles (NPs) have been proposed as carriers for photosensitizers (PS) in photodynamic therapy (PDT), how the designing parameters of nanocarriers affect the final drug efficacy remains unclear. By designing $SiO_2$-PS NPs with specific features (such as enabling PS easy release from the nanocarriers, or introducing plasmonic Au NPs in the vicinity of the PS), and comparing the respective efficacy of PS to that of the conventional dense $SiO_2$-PS NPs (PS were tightly confined into the silica matrix), we identified that both PS trapping-in/releasing from the silica nanocarriers and Au plasmonic effect were responsible for the PS' efficacy variation. The mechanistic study also disclosed that the different NP configurations would affect the cellular death pathway. These understandings provide a general guideline for the design of NPs-based PDT applications.

## Introduction

Photodynamic therapy (PDT) is an effective method for various superficial cancer therapy by combination of administration and irradiation of photosensitizers (PS), which damage the cancer cells by producing reactive oxygen species (ROS)[1-3]. Despite the large number of different PS developed, many of them suffered from inefficient cellular uptake, chemical instability in physiological environment, and consequently low efficacy[4-6]. In recent years, nanoparticles (NPs) have been found to enter cells easily via endocytosis[7, 8], and thus been proposed as effective drug carriers for various PS, aiming at the enhanced drug bioavailability and efficacy.

Silica NPs was one of the most popular candidates as the nanocarriers for PDT applications, due to its easily modifiable surface, excellent chemical stability and low cytotoxicity[9-11]. Nevertheless, it has been found that simply trapping PS in silica NPs seldom resulted in PS efficacy enhancement in PDT[12-14], although enhanced cellular uptake of the PS was always reported[15, 16].

In a typical PDT process, the efficacy of PS is determined by both the type and total amount of produced ROS. One problem associated with PS loaded into NPs is the consequently trapping of the produced ROS—the presence of solid nanocarriers slows down the out-diffusion of the generated ROS. The inhibited ROS escaping from the nanocarriers to cytoplasm would largely reduce their cell killing capability. In this regard, effective release of ROS (or PS themselves) from the silica matrix would improve the drug efficacy. On the other hand, one can expect that increasing generation efficiency of ROS would always contribute to the efficacy enhancement.

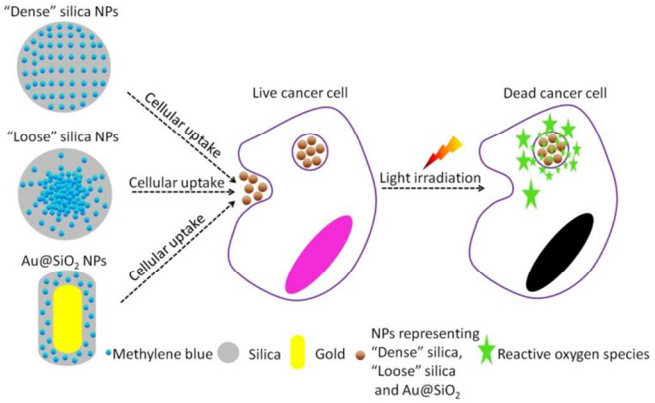


**Fig. 1** Schematic illustration of design of dense $SiO_2$-MB, loose $SiO_2$-MB and Au@($SiO_2$-MB) NPs for performing PDT in vitro.

In the present work, we have designed two specific $SiO_2$-based nanocarriers loading PS to perform PDT in vitro, with one aiming at effective release of the ROS (or PS) upon NPs' cellular uptake, and the other addressing the issue of improving the generation efficiency of ROS. Methylene blue (MB), a typical PS with a wide range of therapeutic applications[17-19], was chosen as a model PDT drug molecule to be incorporated into the corresponding nanocarrier. The design of various nanocarriers for in vitro PDT study was shown in Fig.1. Firstly, MB was uniformly incorporated into the silica matrix using modified Stober's method[20]. This type of conventional $SiO_2$-MB NPs was characterized as tight trapping of MB into the nanocarrier with little drug leakage. We named it as the dense $SiO_2$-MB NPs, and used it as one of the control samples in the following experiments. In the first approach, we fabricated a

special type of "loose" $SiO_2$-MB NPs[21]. Compared to conventional dense silica NPs, the loose $SiO_2$-MB NPs had higher ROS or MB diffusion capability as the NPs themselves would undergo self-decomposition accompanied by facile MB release in physiological environment[21]. In the second approach, we embedded MB in the surface layer of dense silica outside the Au nanorods (NRs) core (denoted as Au@($SiO_2$-MB) NPs), taking the advantage of the surface plasmon enhanced ROS generation. We showed that both approaches improved the drug efficacy of MB. In addition, the detailed mechanisms of the drug efficacy enhancement were discussed.

## Results

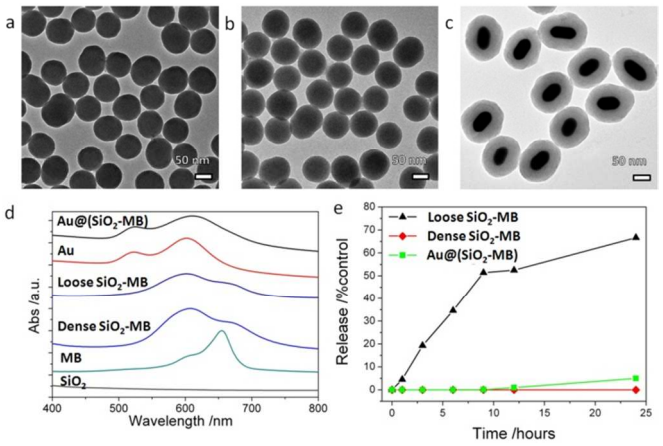


**Fig. 2** Characterization of dense $SiO_2$-MB, loose $SiO_2$-MB and Au@($SiO_2$-MB) NPs. Low magnification TEM images of (a) dense $SiO_2$-MB NPs, (b) loose $SiO_2$-MB NPs and (c) Au@($SiO_2$-MB) NPs; (d) Absorption spectra taken from $SiO_2$ NPs, MB alone, dense $SiO_2$-MB, loose $SiO_2$-MB, Au NRs and Au@($SiO_2$-MB) NPs in aqueous solution ([MB]= 5 μM for all samples); (e) Evolution of the MB released from the NPs as a function of the immersing duration in PBS at 37 °C.

The as-synthesized dense $SiO_2$-MB NPs and loose $SiO_2$-MB NPs were all spherical in shape with an average diameter ~80 nm (Fig. 2a-b). The as-synthesized Au@($SiO_2$-MB) NPs were uniform with a core/shell morphology (Fig. 2c). The Au NRs core had an average diameter of ~40 nm and an aspect ratio close to 2, and the MB containing silica shell appeared uniform with a thickness of ~40 nm. Evidence of successful MB incorporation into the $SiO_2$ matrix can be found in the absorption spectra taken from these samples (Fig. 2d). $SiO_2$ alone has little absorption in the wavelength range of 400-800 nm. MB itself had two absorption peaks at 665nm and 600nm, corresponding to its monomer and dimer absorption, respectively (Fig. 2d). When incorporated into the $SiO_2$, its dimer form was significantly increased due to MB aggregation[21]. The Au NRs itself had two plasmonic absorption peaks with the transverse mode occurring at ~522 nm, and longitudinal mode at longer wavelength, which was tunable (~600 nm in the present case) by varying the aspect ratio of NRs. Comparing to that of the Au NRs alone, incorporating MB into the $SiO_2$ shell (in the Au@($SiO_2$-MB) NPs) only broadened the Au longitudinal SPR, without much affecting the spectrum line shape. This was mainly due to the position overlap between the Au longitudinal SPR and the MB dimer absorption[20]. We then investigated the release behavior of MB molecules from these nanocarriers in phosphate buffered saline (PBS, pH~7.4) at 37 °C (mimicking the physiological condition). One could observe that nearly 60% MB was released from the loose $SiO_2$-MB NPs after 24 hours' incubation, while only less than 5% MB escaped from the dense $SiO_2$-MB or Au@($SiO_2$-MB) NPs.

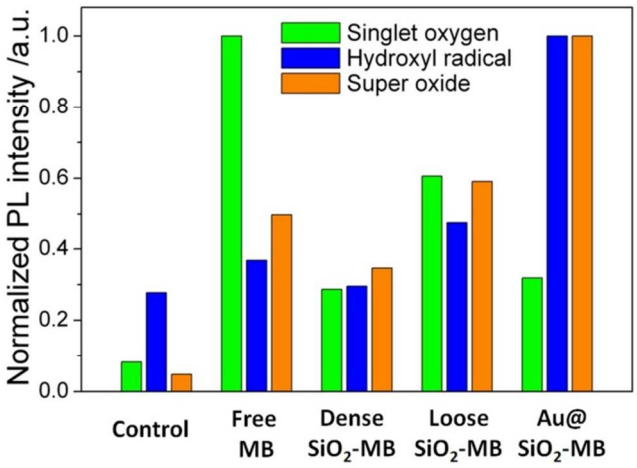


**Fig. 3** Quantitative comparison of various ROS generation including singlet oxygen, hydroxyl radical and super oxide in various MB loaded NPs in aqueous solution. The amount of specific ROS was represented by the height of the fluorescent peak of various ROS detection dye in Fig. S1.

Generally speaking, there were two major types of ROS generated by light irradiation of PS (MB in the present case), i.e., Type I and Type II ROS. Type I ROS was known as the free radicals, including primary species such as superoxide and secondary species such as hydroxyl radicals, while Type II ROS mainly referred to singlet oxygen[22]. Since the cell responded differently to different types of ROS, we compared the major types and the corresponding amount of generated ROS by free MB or MB loaded into various nanocarriers in a semi-quantitative manner in aqueous solution.

Singlet oxygen sensor green (SOSG) was chosen as the detection agent for the generated singlet oxygen[23], which amount was represented by the height of the fluorescent peak of SOSG at 525 nm. For the control sample (only SOSG in aqueous solution), a weak signal was observed and can be attributed to the background signal of singlet oxygen in the solution. An obvious fluorescent peak at 525 nm with high intensity (Fig. S1) could be seen after 20 minutes' irradiation of the free MB containing sample. As a comparison, the amount of singlet oxygen generated from loose $SiO_2$-MB NPs was barely half of that from free MB, while the amount of the singlet oxygen detected in dense $SiO_2$-MB NPs was similar to that from Au@($SiO_2$-MB) NPs, it was merely half of that produced from loose $SiO_2$-MB NPs (green bar in Fig. 3).

The generated hydroxyl radicals and superoxide were measured using detection dye terephthalic acid (TA)[24] and

dihydroethidium (DHE)[25], respectively. An obvious fluorescent peak at 425 nm (Fig. S1), which indicated the presence of hydroxyl radicals, could be observed in solution containing Au@($SiO_2$-MB) NPs after light irradiation for 20 minutes. Such peak can also been observed in all other samples, but with all of their intensities only slightly higher than that of the control sample (blue bar in Fig. 3), indicating little generation of hydroxyl radicals from those samples without Au NRs core. For superoxide radicals detected using DHE, both free MB, loose $SiO_2$-MB, dense $SiO_2$-MB, and Au@($SiO_2$-MB) NPs showed distinct fluorescent peak values at 586 nm (Fig. S1), with the order of the peak intensity as: Au@($SiO_2$-MB) NPs>loose $SiO_2$-MB>free MB>dense $SiO_2$ MB (orange bar in Fig.3). We have also investigated the ROS produced by Au@SiO2 NPs, and found the results were similar to those of the control sample, i.e., aqueous solution containing ROS detection dyes only (Results not shown here).

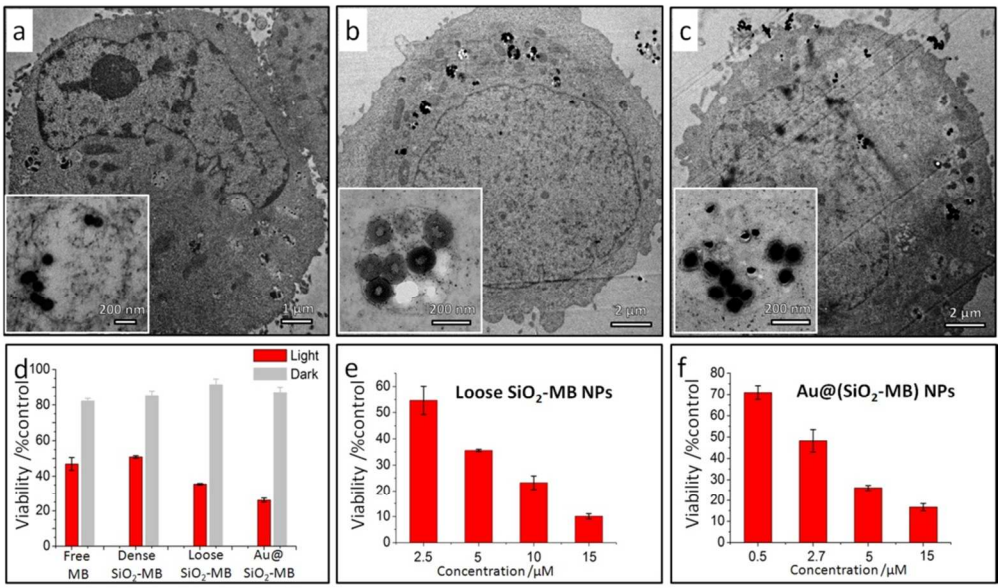


**Fig. 4** Intracellular locations of various MB loaded NPs upon cellular uptake, and the efficacy of free MB or various MB loaded NPs when performing PDT in Vitro. TEM images showing a typical HepG2 cell after being incubated with (a) dense $SiO_2$-MB, (b) loose $SiO_2$-MB and (c) Au@($SiO_2$-MB) NPs for 24 hours, insert is the magnified TEM image of one selected vesicle. (d) MTT results of the HepG2 cells treated with pure MB, dense $SiO_2$-MB, loose $SiO_2$-MB and Au@($SiO_2$-MB) NPs for 24 hours (the concentration of MB was fixed as 5 μM in all samples). MB concentration dependence of the HepG2 cells viability when being incubated with (e) loose $SiO_2$-MB NPs and (f) Au@($SiO_2$-MB) NPs for 24 hours, the feeding concentration of the NPs was kept the same for all experiments. All data were shown as mean ± SD (from three independent experiments) and significantly different ($p < 0.05$) from control (analyzed by Student's t test).

In vitro results showed that all kinds of MB loaded NPs, including the dense $SiO_2$-MB, loose $SiO_2$-MB and Au@($SiO_2$-MB) NPs entered the cells easily (Fig. 4a-c). The fact that these nanocarriers were always found in membrane bounded vesicles (as shown in the insert of Fig. 4a-c) after cellular uptake suggested endocytosis as the major route for NPs' cellular entry[26]. For the PDT experiments carried out in vitro, the efficacy of free MB or MB loaded in various nanocarriers were firstly evaluated using MTT assay at concentration of [MB] = 5μM (a value ~ IC50 of free MB, see Fig. S2) in HepG2 cells (Fig. 4d). Low cytotoxicity (~85% viability) was observed for all samples in dark. After light irradiation for 20 minutes, the cell viability dropped to 47% for free MB, 51% for dense $SiO_2$-MB, 35% for loose $SiO_2$-MB and 26% for Au@($SiO_2$-MB) NPs treated samples (Fig. 4d). The concentration dependent effect of both loose $SiO_2$-MB and Au@($SiO_2$-MB) NPs treated cells were also demonstrated (Fig. 4e and Fig. 4f). Comparing to free MB alone (IC50 was 4.70 μM (Fig. S2)), both the loose $SiO_2$-MB and the Au@($SiO_2$-MB) NPs largely enhanced MB efficacy with IC50 of 2.63 μM (Fig. 4e) and 2.59 μM (Fig. 4f), respectively.

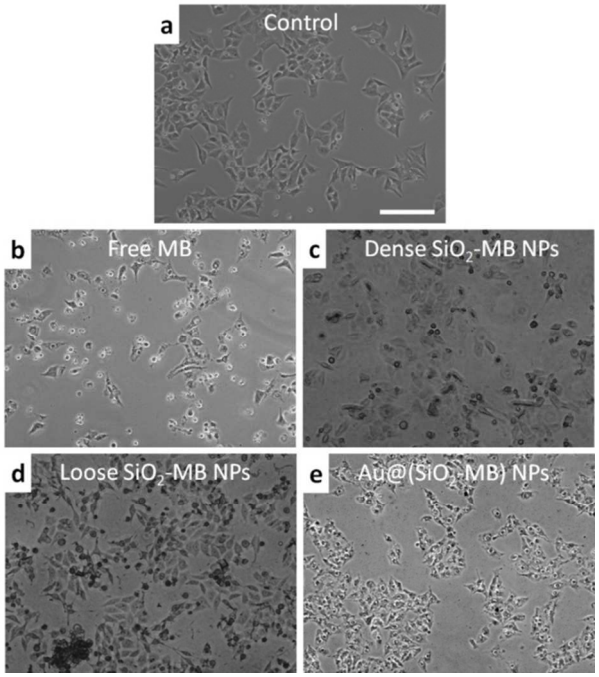

**Fig. 5** Morphology change of cells treated with various samples after in vitro PDT treatment. Light microscopy images of HepG2 cells treated with (a) medium (control), (b) free MB and (c) dense $SiO_2$-MB, (d) loose $SiO_2$-MB and (e) Au@($SiO_2$-MB) NPs for 24 hours (the concentration of MB was fixed as 5 μM for all samples), followed by the light irradiation for 20 minutes and further incubation with NP-free medium for another 24 hours. The scale bar is 100 μm.

The presence of different types of dominant ROS suggested different death pathways for the cells after their incubation with free MB or MB loaded NPs (upon light irradiation). It was known that singlet oxygen was more likely to direct cells to apoptosis (including early and late apoptosis)[27, 28], while free radicals (including both hydroxyl radicals and superoxide) would lead cells to necrosis[29]. In addition, higher ROS level was also more likely to induce necrosis rather than apoptosis[30]. As MTT assay only disclosed the overall cell viability, we took another approach to evaluate the cell death pathway. As the morphological features of the cells would vary when they underwent either apoptosis or necrosis[31], we compared the cell morphology after their being treated with free MB and MB loaded NPs using light microscopy. In free MB, dense $SiO_2$-MB NPs and loose $SiO_2$-MB NPs treated samples, cells with shrinking membrane as well as their detaching from the substrate were commonly observed, which features were consistent with the apoptosis pattern[31] (Fig. 5b-d). As a comparison, most of the cells remained being attached to the substrate but with massive production of bubbles when treated with Au@($SiO_2$-MB) NPs (Fig. 5e). The bubble formation, which was a features of necrosis[31], can be observed in cells treated with Au@($SiO_2$-MB) NPs after only a few minutes' light irradiation (Fig. S3). These light microscopy results indicated that apoptosis was dominant in cells treated with free MB, dense $SiO_2$-MB NPs and loose $SiO_2$-MB NPs, while necrosis served as the predominant death route for Au@($SiO_2$-MB) NPs treated cell samples.

## Discussions

The experimental results suggested that trapping MB into dense $SiO_2$ matrix suppressed all types of generated ROS (Fig. 3). This was mainly due to the difficulty in ROS's out-diffusion from the NPs—MB was trapped in the dense $SiO_2$ matrix, and ROS was always firstly generated in the vicinity of MB and then diffuse to elsewhere[20]. This was particularly important when the life time of a specific ROS was short, such as the singlet oxygen and hydroxyl radical[32]. Compared to dense $SiO_2$-MB NPs, loose $SiO_2$-MB NPs showed enhanced generation of all types of ROS examined. This was caused by the loose and fragmentable features of the loose $SiO_2$-MB NPs[21], resulting in easier diffusion of the generated ROS.

However, one shall notice that the amount of singlet oxygen generated by the loose $SiO_2$-MB NPs was also lower than that of free MB, being opposite to the case of hydroxyl radical and superoxide. This was not too surprising, as the incorporation of MB into $SiO_2$ matrix would promote the MB dimer formation at the expense of MB monomer[33]. While MB monomer mainly produced singlet oxygen under light irradiation, the excitation of the dimer led to large amount of free radicals (e.g., hydroxyl radical and superoxide) generation[34]. In fact, this phenomenon held for all MB-loaded $SiO_2$ NPs as shown in Fig. 3. Comparing to singlet oxygen, which mainly caused apoptosis, the free radicals (e.g., hydroxyl radicals and superoxide) were more likely to cause necrosis, and thus acted as more effective agents for cell killing in PDT[29]. It was also important to note that apoptosis (major pattern of cell death in free MB treated samples) was not an effective cell death pathway, as it did not necessarily lead to cell death[35]. In addition, cancer cells may develop resistance to apoptosis[36]. These then provided a reasonable explanation to the observed cell viability difference (Fig. 4d), i.e., the loose $SiO_2$-MB NPs showed the highest cell death rate when compared to free MB and dense $SiO_2$-MB NPs, although the amount of singlet oxygen generated by loose $SiO_2$-MB NPs was merely half of that of the free MB.

Although the MB (or generated ROS) was also trapped in the case of Au@($SiO_2$-MB) NPs, such $SiO_2$ shell was quite thin (~40 nm). On the other hand, the introduction of Au NRs brought in plasmonic effect. With the MB dimer absorption matching the surface plasmon resonance energy of the Au core (Fig. 2d) and the spatial confinement of MB in the vicinity of Au, MB absorption and thus the corresponding generation efficiency of ROS was significantly increased due to the plasmonic enhancement effect[20], especially for the type I ROS (i.e. hydroxyl radicals and superoxide) (Fig. 3). Here one can exclude contribution of Au @$SiO_2$ only, as we found that the ROS produced by Au@$SiO_2$ NPs was similar to those of the control sample, i.e., aqueous solution containing ROS detection dyes only. Neither did the presence of Au@$SiO_2$ decrease the cell viability when irradiated by light at the described experimental conditions (Results not shown here). The enhanced generation of type I ROS due to Au plasmonic effect was responsible for the most effective PDT in vitro (Fig. 4d). Therefore, the observed cell viability decrease in Au@($SiO_2$-MB) NPs treated samples resulted from both plasmonic enhanced generation of ROS, and the predominant type I ROS produced by MB dimers.

## Conclusions

In conclusion, we found that incorporation of MB into silica matrix would bring in a number of advantages, i.e., dominance of dimmer instead of monomer would produce predominant type I ROS, which were more efficient agents responsible for cell death. Nevertheless, the traditional dense silica nanocarriers would reduce the ROS production due to their difficult diffusion out of silica matrix. We tackled this problem by designing loose $SiO_2$-MB NPs, in which facile diffusion of MB and generated ROS was realized via self-decomposition of such nanocarriers, and an enhanced drug efficacy was demonstrated. We also showed that increasing the generation efficiency of ROS by introducing Au plasmonic effect served as an alternative route for enhanced drug efficacy. Such mechanisms provided a general guideline for the optimum design of NPs-based drug delivery for PDT.

## Experimental

**Preparation of various MB loaded NPs**

The loose $SiO_2$-MB NPs were synthesized using conventional method[21] with modified parameters. In a typical procedure, 2.5mg MB was firstly added to a mixture of 75 ml ethanol with 3.4 ml 25% ammonia-water solution, after that 0.08 ml TEOS was added. The loose SiO2-MB NPs were obtained after 24 hours' stirring, and washed several times before their being dried. The dense $SiO_2$-MB NPs were synthesized using published method[21], briefly, 2.5 mg of MB was added to a mixture of 50 ml ethanol with 5 ml 25% ammonia-water solution, after that 0.2 ml TEOS was added. The ammonia amount is 2.27%vol., which is more than double of that in synthesizing self-decomposable NPs (<1.08%vol.). Such recipe was known to generate dense $SiO_2$-MB NP, in which the MB can be stably trapped in $SiO_2$.

The growth of the Au NRs was firstly conducted using a seed-mediated method[20]. The as-grown NRs can be shortened by oxidation to the required aspect ratio. Pegylation of Au NR (40 ml) was realized by mixing them with freshly prepared aqueous mPEG-SH solution (1 mM, 2 ml; NANOCS, America) in 30 $^oC$ water bath overnight. Growth of the Au@($SiO_2$-MB) NPs was similar to that of Au@$SiO_2$ NPs reported in the literature[37]. In a typical procedure, 7.5 ml as-prepared PEG-stabilized Au NRs (in ethanol) were mixed with 2.3 ml deionized H2O and 0.15 ml 30% ammonia-water solution, after that 50 μl MB stock solution (10 mM in ethanol) was added before 20 μl TEOS was finally introduced. The resulted NPs were washed and dried at 65 $^oC$ for further use.

The general morphology, size, and the size distribution of various NPs were characterized using transmission electron microscopy (TEM, PhilipsCM120). All of the UV/Vis absorption spectra were acquired using HitachiU-3501UV-visible-NIR spectrophotometer.

**Quantifying the ROS generation of various MB loaded NPs in cuvette**

To study ROS generation in cuvette, three different reagents were selected to detect the singlet oxygen (singlet oxygen sensor green (SOSG), Ex: 488 nm), hydroxyl radical (terephthalic acid (TA), Ex: 315 nm) and superoxide (dihydroethidium (DHE), Ex: 470 nm), respectively. The free MB, dense $SiO_2$-MB, loose $SiO_2$-MB and Au@($SiO_2$-MB) NPs were respectively dispersed in cuvette with deionized water, followed by addition of proper amount of the specific ROS detection dye, and then irradiated with 590 nm LED light for 20 minutes. Finally, the fluorescence signals of different ROS detection dyes in the cuvette were measured by a fluorescence spectrophotometer (Hitachi, FL7000). In all experiments, deionized water containing only the corresponding ROS detection dyes were used as the controls. The fluorescence intensity of various ROS detection dyes was finally normalized by the concentration of MB (The concentration of MB was fixed as 5 μM in all samples.).

**Introduce various MB loaded NPs to the cells for performing PDT in vitro**

HepG2, the human liver carcinoma cells, were cultured in Dulbecco's modified Eagle's medium (DMEM), supplemented 10% heat-inactivated Fetal bovine serum (FBS), 2.0 g/L sodium bicarbonate, 0.1 g/L streptomycin sulfate, 0.06 g/L penicillin G and 5.958 g/L HEPES. The cells were maintained in a standard, cell culture incubator at 37 $^oC$ in a humidified atmosphere with 5 % $CO_2$.

All of the NPs were sterilized by steaming at 115 $^oC$ (NPs in powder form) for 2 hours, before they were dispersed in the medium and introduced to the cells, which had already been seeded and incubated for 24 hours. The concentration of NPs used in this study can be represented by that of Au NRs, which was calculated to be 0.34nM from its UV/Vis absorption5.

A home-built 590 nm LED (emission profile is shown in Fig. S4) was employed for the in vitro PDT study. The LED was aligned directly under the sample wells (96-well plates) to obtain uniform irradiation of the cells. The power density of the LED is 5 $mW/cm^{-2}$, which is too weak to cause any irradiation damage to the cells (Fig. S5).

**Characterizations of the cells**

For all transmission electron microscopy studies, the NP-fed cells were fixed with typical procedures published elsewhere[26]. Microtome (Leica, EM UC6) was then used to cut the cured cell cube (in Spurr resin (Electron microscopy sciences, USA)) into thin slices (70-90 nm in thickness). The samples were collected on 300-mesh copper TEM grids for observation.

The cell viability was measured 24 hours after irradiation using MTT assay. The 24 hours delay was designed to account for both apoptosis and necrosis mechanisms of cell death7. The significance of all data was determined by Student's t-test for all in vitro studies, $p<0.05$ was deemed as significant for all data compared to control.

The morphology change of HepG2 cells was observed with light microscope (Olympus CKX41, Japan). The cells were initially seeded in a 6 well plate at the initial density of $1\times10^5$ /ml (2 ml) in DMEM medium with 10% FBS. After allowing 24 hours for cell attachment, original medium were discard and the free MB/MB loaded NPs containing medium were added to the cell samples ([MB] =5 μM) dosing for 24 hours. Finally, the cell was observed 24 hours after irradiation using light microscope with a 10 × objective lens.

## Acknowledgements

The authors are grateful for financial support from CUHK direct grant (Project No. 4053074).

[a]*Department of Physics, The Chinese University of Hong Kong, Shatin, New Territories, Hong Kong. E-mail: liquan@phy.cuhk.edu.hk*
[b]*School of Biomedical Sciences, Faculty of medicine, The Chinese University of Hong Kong, Shatin, New Territories, Hong Kong.*
[†]*These authors contributed equally to this work.*

Electronic Supplementary Information (ESI) available: [details of any supplementary information available should be included here]. See DOI: 10.1039/b000000x/

## Reference

1. P. Huang, J. Lin, X. S. Wang, Z. Wang, C. L. Zhang, M. He, K. Wang, F. Chen, Z. M. Li, G. X. Shen, D. X. Cui and X. Y. Chen, *Adv. Mater.*, 2012, **24**, 5104-5110.
2. D. E. Dolmans, D. Fukumura and R. K. Jain, *Nat. Rev. Cancer*, 2003, **3**, 380-387.
3. C. A. Robertson, D. H. Evans and H. Abrahamse, *J. Photochem. Photobiol. B*, 2009, **96**, 1-8.
4. P. Huang, J. Lin, D. Yang, C. Zhang, Z. Li and D. Cui, *J. Control. Release*, 2011, **152 Suppl 1**, e33-34.
5. J. Lin, S. Wang, P. Huang, Z. Wang, S. Chen, G. Niu, W. Li, J. He, D. Cui, G. Lu, X. Chen and Z. Nie, *Acs Nano*, 2013, **7**, 5320-5329.
6. H. Y. Yang, F. Y. Wang and Z. Y. Zhang, *Dyes Pigments*, 1999, **43**, 109-117.
7. W. Jiang, B. Y. S. Kim, J. T. Rutka and W. C. W. Chan, *Nat. Nanotechnol.*, 2008, **3**, 145-150.
8. M. E. Davis, Z. G. Chen and D. M. Shin, *Nat. Rev. Drug Discov.*, 2008, **7**, 771-782.
9. H. L. Tu, Y. S. Lin, H. Y. Lin, Y. Hung, L. W. Lo, Y. F. Chen and C. Y. Mou, *Adv. Mater.*, 2009, **21**, 172-+.
10. P. Couleaud, V. Morosini, C. Frochot, S. Richeter, L. Raehm and J. O. Durand, *Nanoscale*, 2010, **2**, 1083-1095.
11. P. Huang, J. Lin, S. J. Wang, Z. J. Zhou, Z. M. Li, Z. Wang, C. L. Zhang, X. Y. Yue, G. Niu, M. Yang, D. X. Cui and X. Y. Chen, *Biomaterials*, 2013, **34**, 4643-4654.
12. V. Simon, C. Devaux, A. Darmon, T. Donnet, E. Thienot, M. Germain, J. Honnorat, A. Duval, A. Pottier, E. Borghi, L. Levy and J. Marill, *Photochem. Photobiol.*, 2010, **86**, 213-222.
13. B. Zhao, J. J. Yin, P. J. Bilski, C. F. Chignell, J. E. Roberts and Y. Y. He, *Toxicol. Appl. Pharmacol.*, 2009, **241**, 163-172.
14. C. Compagnin, L. Bau, M. Mognato, L. Celotti, G. Miotto, M. Arduini, F. Moret, C. Fede, F. Selvestrel, I. M. R. Echevarria, F. Mancin and E. Reddi, *Nanotechnology*, 2009, **20**.
15. I. I. Slowing, J. L. Vivero-Escoto, C. W. Wu and V. S. Y. Lin, *Adv. Drug Deliver. Rev.*, 2008, **60**, 1278-1288.
16. I. I. Slowing, B. G. Trewyn, S. Giri and V. S. Y. Lin, *Adv. Funct. Mater.*, 2007, **17**, 1225-1236.
17. B. Coulibaly, A. Zoungrana, F. P. Mockenhaupt, R. H. Schirmer, C. Klose, U. Mansmann, P. E. Meissner and O. Muller, *PLoS One*, 2009, **4**, e5318.
18. M. Oz, D. E. Lorke and G. A. Petroianu, *Biochem. Pharmacol.*, 2009, **78**, 927-932.
19. R. H. Schirmer, H. Adler, M. Pickhardt and E. Mandelkow, *Neurobiol Aging*, 2011, **32**.
20. Z. Chu, C. Yin, S. Zhang, G. Lin and Q. Li, *Nanoscale*, 2013, **5**, 3406-3411.
21. S. L. Zhang, Z. Q. Chu, C. Yin, C. Y. Zhang, G. Lin and Q. Li, *J. Am. Chem. Soc.*, 2013, **135**, 5709-5716.
22. M. Valko, D. Leibfritz, J. Moncol, M. T. D. Cronin, M. Mazur and J. Telser, *Int. J. Biochem. Cell B*, 2007, **39**, 44-84.
23. C. Flors, M. J. Fryer, J. Waring, B. Reeder, U. Bechtold, P. M. Mullineaux, S. Nonell, M. T. Wilson and N. R. Baker, *J. Exp. Bot.*, 2006, **57**, 1725-1734.
24. K. Ishibashi, A. Fujishima, T. Watanabe and K. Hashimoto, *Electrochem. Commun.*, 2000, **2**, 207-210.
25. Y. Zhang, K. Aslan, M. J. R. Previte and C. D. Geddes, *Appl. Phys. Lett.*, 2007, **91**.
26. Z. Q. Chu, Y. J. Huang, Q. Tao and Q. Li, *Nanoscale*, 2011, **3**, 3291-3299.
27. I. E. Kochevar, M. C. Lynch, S. G. Zhuang and C. R. Lambert, *Photochem. Photobiol.*, 2000, **72**, 548-553.
28. C. P. Lin, M. C. Lynch and I. E. Kochevar, *Exp. Cell Res.*, 2000, **259**, 351-359.
29. Y. H. Kim, E. Y. Kim, B. J. Gwag, S. Sohn and J. Y. Koh, *Neuroscience*, 1999, **89**, 175-182.
30. S. V. Lennon, S. J. Martin and T. G. Cotter, *Cell Proliferat.*, 1991, **24**, 203-214.
31. S. Rello, J. C. Stockert, V. Moreno, A. Gamez, M. Pacheco, A. Juarranz, M. Canete and A. Villanueva, *Apoptosis*, 2005, **10**, 201-208.
32. L. M. Rossi, P. R. Silva, L. L. R. Vono, A. U. Fernandes, D. B. Tada and M. S. Baptista, *Langmuir*, 2008, **24**, 12534-12538.
33. D. B. Tada, L. L. R. Vono, E. L. Duarte, R. Itri, P. K. Kiyohara, M. S. Baptista and L. M. Rossi, *Langmuir*, 2007, **23**, 8194-8199.
34. H. C. Junqueira, D. Severino, L. G. Dias, M. S. Gugliotti and M. S. Baptista, *Phys. Chem. Chem. Phys.*, 2002, **4**, 2320-2328.
35. B. Fadeel, B. Gleiss, K. Hogstrand, J. Chandra, T. Wiedmer, P. J. Sims, J. I. Henter, S. Orrenius and A. Samali, *Biochem. Biophys. Res. Commun.*, 1999, **266**, 504-511.
36. A. Ashkenazi, *Nat. Rev. Cancer*, 2002, **2**, 420-430.
37. C. Fernandez-Lopez, C. Mateo-Mateo, R. A. Alvarez-Puebla, J. Perez-Juste, I. Pastoriza-Santos and L. M. Liz-Marzan, *Langmuir*, 2009, **25**, 13894-13899.

**Table of contents:**

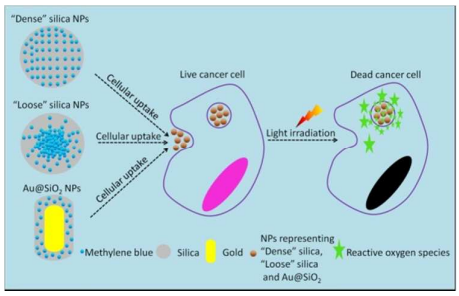


The current work revealed how the designing parameters of nanocarriers affect the drug efficacy in photodynamic therapy.